iScience

CellPress
OPEN ACCESS

Article

General method to stabilize mesophilic proteins in hyperthermal water

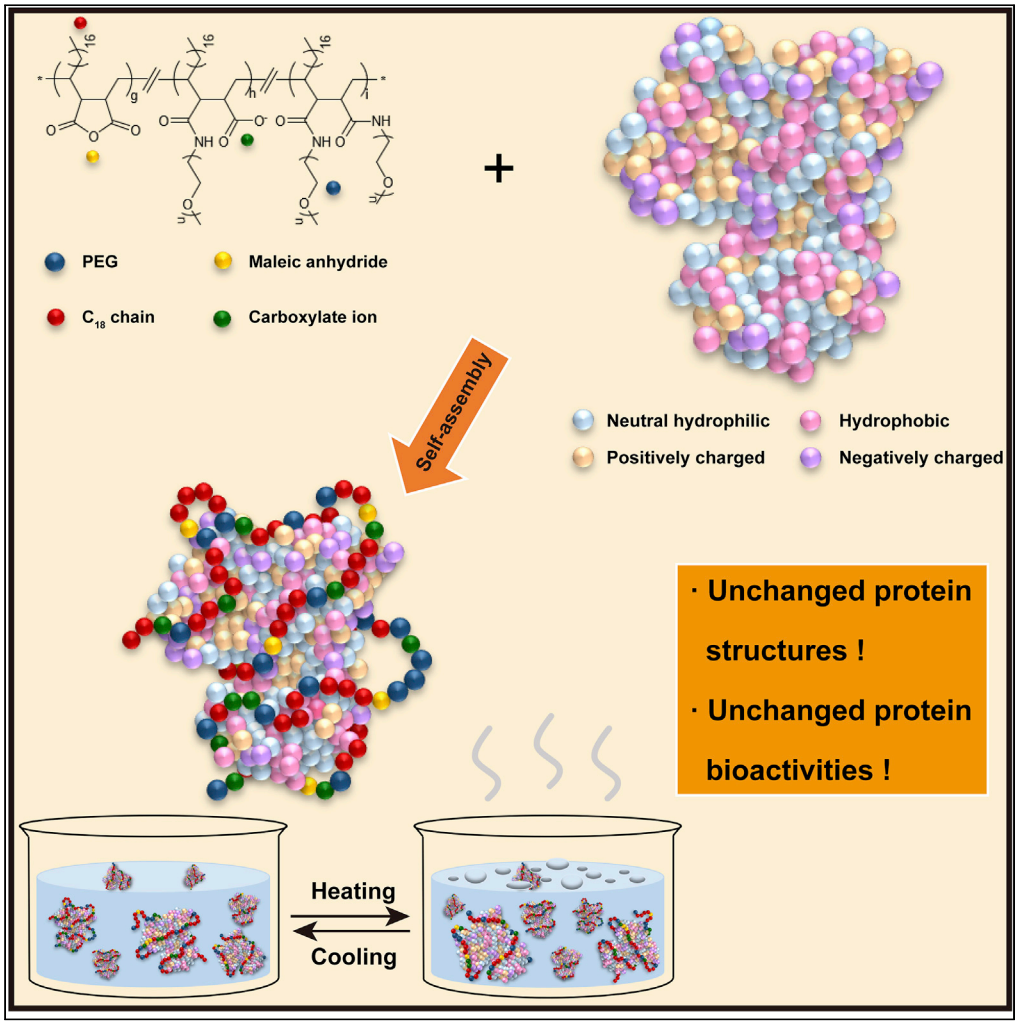

Xiaoqian Xin, Youwei Xu, Hu Shi, Xiaowen Liu

xwliu231@jnu.edu.cn

Highlights

Preserving bioactivities of proteins in hyperthermia water is promising.

Amphiphilic polymers could protect mesophilic proteins even in boiling water.

Mesophilic proteins protected by amphiphilic polymers show dramatically increased T_m.

The method offers application prospect for vaccine storage and enzyme engineering.

Xin et al., iScience 24, 102503
May 21, 2021
https://doi.org/10.1016/j.isci.2021.102503

iScience

CellPress
OPEN ACCESS

Article

General method to stabilize mesophilic proteins in hyperthermal water

Xiaoqian Xin,[1] Youwei Xu,[2] Hu Shi,[3] and Xiaowen Liu[1,4,*]

SUMMARY

The stability of protein structures and biological functions at normal temperature is closely linked with the universal aqueous environment of organisms. Preserving bioactivities of proteins in hyperthermia water would expand their functional capabilities beyond those in native environments. However, only a limited number of proteins derived from hyperthermophiles are thermostable at elevated temperatures. Triggered by this, here we describe a general method to stabilize mesophilic proteins in hyperthermia water. The mesophilic proteins, protected by amphiphilic polymers with multiple binding sites, maintain their secondary and tertiary structures after incubation even in boiling water. This approach, outside the conventional environment for bioactivities of mesophilic proteins, provides a general strategy to dramatically increase the T_m (melting temperature) of mesophilic proteins without any changes to amino sequences of the native proteins. Current work offers a new insight with protein stability engineering for potential application, including vaccine storage and enzyme engineering.

INTRODUCTION

Most organisms only survive at low or moderate temperatures in aqueous environment, as these temperatures are the optimal working conditions for mesophilic proteins. High temperatures can induce denaturation and aggregation of mesophilic proteins (Chang and Bowie, 2014; Leuenberger et al., 2017; Mahler et al., 2009; Watson et al., 2018), limiting the boundary of their functions. Stabilizing proteins out of their native physiological environments would generate extraordinary achievements. Proteins as biocatalyst retain their functions at higher temperatures than their physiological temperatures would yield higher reaction rates (Arnold and Volkov, 1999; Ni et al., 2018; Schoene et al., 2014; Vieille and Zeikus, 2001). Preserving protein vaccines current with cold-chain requirement at room or higher temperatures for longer duration would extend the vaccine potency in developing countries (Levin et al., 2007; Ohtake et al., 2011; Wang et al., 2012). In addition, enhancing the thermostability of proteins at elevated temperatures probably provides the clue that the living system could be different from the current standard on the earth (Lopez-Garcia et al., 2015; Martin et al., 2008; Rothschild and Mancinelli, 2001). Despite their great potential application and years of effort, there has been very limited strategies to stabilize mesophilic proteins out of their native environments without structure and function compromised (Kazlauskas, 2018).

A minority of thermophilic proteins from extremophilic organisms (e.g. archaea) could retain their structures and functions at elevated temperatures (Razvi and Scholtz, 2006; Rothschild and Mancinelli, 2001). In addition, a single or multiple mutations can enhance the thermostability of the artificial engineered proteins (Imanaka et al., 1986; Matthews et al., 1987) by sequence comparison of the mesophilic proteins and their thermophilic counterparts, nevertheless confining to the engineering of proteins that related with their thermophilic counterparts. Chemical engineering methodologies, including covalent conjugation or non-covalent encapsulation, are also useful for protein stabilization. Protein saccharides/PEG conjugates can lead to an enhancement of protein functionality beyond normal physicochemical conditions (pH, temperature, and stress) for proteins (Akhtar and Ding, 2017; Baker et al., 2018; Cummings et al., 2014; Mensink et al., 2017). Protein complexes fabricated by self-assembly of proteins with amphiphilic polyanhydrides, carboxymethylcellulose, or surfactants could also improve their stability in pharmaceutical or beverage applications (Akram et al., 2017; Satish et al., 2019; Torres et al., 2007; Wagoner and Foegeding, 2017). Although these excipients stabilize proteins, long-term stabilization of mesophilic proteins in hyperthermal water remains a significant challenge.

[1]Clinical Translational Center for Targeted Drug, School of Medicine, Jinan University, Guangzhou 510632, China

[2]Shanghai Institute for Advanced Immunochemical Studies, ShanghaiTech University, Shanghai 201210, China

[3]School of Chemistry and Chemical Engineering, Institute of Molecular Science, Shanxi University, Taiyuan 030006, China

[4]Lead contact

*Correspondence: xwliu231@jnu.edu.cn

https://doi.org/10.1016/j.isci.2021.102503

Mirrored by the sequence analysis of thermophilic proteins (Razvi and Scholtz, 2006; Vieille and Zeikus, 2001) and principle of de novo protein design (Huang et al., 2016; Koepnick et al., 2019; Moffet and Hecht, 2001; Thomas and Elcock, 2004), several subunits within proteins, such as hydrophobic interactions, hydrogen bonds, and ion pairs, are documented to play dominant roles for the protein thermostability (Liu et al., 2016; Monteith et al., 2015; Mossuto et al., 2011; Scirè et al., 2008; Xiao et al., 2013). Considering that polymers could be synthesized at similar molecular scale and mimicked the diverse binding sites as that of proteins, an artificial polymer with the balanced hydrophobic or hydrogen-bond binding sites may enhance its interactions with mesophilic proteins (Hannink et al., 2001; Ke et al., 2019; Lawrence et al., 2014; Ma et al., 2020). Inspired by this, we proposed that potential binding sites (hydrophobic chains and hydrophilic groups) collectively fused in one amphiphilic polymer might strengthen their interactions with mesophilic proteins for thermal protection. For the purpose, we synthesized a series of amphiphilic polymers (P_xM_y) with PEG and C_{18} chains for encapsulation and protection of mesophilic proteins; the optimal amphiphilic polymers (P_1M_5, P_1M_{10}) with balanced hydrophobic chains and hydrophilic groups could stabilize mesophilic proteins with retained secondary and tertiary structures in hyperthermal water, presenting a general method to stabilize mesophilic proteins with promising applications, such as vaccine storage without cold-chain requirement and enzyme engineering at high temperatures.

RESULTS AND DISCUSSION

Preparation of amphiphilic polymers to encapsulate proteins

We tested a diverse of mesophilic proteins with different characteristics, including BSA (BSA, isoelectric point 5.82, MW 66.4 kDa), transferrin (TRF, isoelectric point 6.7, MW 75.2 kDa), myohemoglobin (MB, isoelectric point 7.2, MW 17.1 kDa), and insulin (INS, isoelectric point 5.22, MW 5.8 kDa) (Figure 1A). We synthesized a series of amphiphilic polymers anchored with hydrophobic and hydrophilic binding sites (Liu et al., 2011). Various densities of PEG (PEG: monomer = 2:1, 1:1, 1:2, 1:5, 1:10, respectively) were conjugated to the hydrophobic polymers (poly(maleic anhydride-alt-1-octadecene), $PMHC_{18}$) to tailor the hydrophilicity of polymers, generating amphiphilic polymers (P_2M_1, P_1M_1, P_1M_2, P_1M_5, and P_1M_{10}) (Figures 1B, S1, and S2). After the conjugation, these polymers were anchored with potential binding sites including hydrophobic C_{18} chains to tailor the hydrophobicity for protein compaction and stabilization and hydrophilic PEG chains to shield and stabilize proteins. These binding sites are hypothesized to enhance their non-covalent interactions with mesophilic proteins by a chaperone-like effect (Figure 1C), thus protecting mesophilic proteins from denaturation and aggregation at elevated temperatures (Figure 1D).

We initially experimentally examined if these amphiphilic polymers could encapsulate mesophilic proteins. BSA as the first model protein and P_xM_y amphiphilic polymers (x = 2, 1; y = 1, 2, 5, 10) were cosolubilized in deionized water for encapsulation of BSA, purified by dialysis and lyophilized. All five polymers (P_2M_1, P_1M_1, P_1M_2, P_1M_5, and P_1M_{10}) showed high encapsulation efficiency (EE) and loading content (LC) of BSA (Figures S3A and S3B). Transmission electron microscopy (TEM) and dynamic light scattering (DLS) measurements revealed that P_xM_y@BSA form nanocomplexes with diameter around 20 nm (Figures S3C and S6). Fourier transform infrared spectroscopy (FTIR) (Eyles et al., 2000; Kong and Yu, 2007) of P_xM_y@BSA showed amide I at 1655 cm^{-1}, amide II band at 1535 cm^{-1}, amide band A at 3500 cm^{-1}, and amide band B at 3065 cm^{-1} (Figures 2A and S4), respectively. The characteristic peaks of P_xM_y@BSA and their relative intensities are consistent with that of native BSA, indicating unvaried structures of BSA after encapsulation with amphiphilic polymers. In addition, narrower peak half-widths for P_1M_5@BSA and P_1M_{10}@BSA were observed compared with that of native BSA, signifying more stable helices (Barth, 2007; Kong et al., 2018) possibly due to the protein intermolecular crowding and confinement generated from polymer encapsulation.

Amphiphilic polymers stabilize proteins in hyperthermia water

To test our hypothesis whether P_xM_y polymers are capable of stabilizing mesophilic proteins in hyperthermia water, we redissolved the five lyophilized P_xM_y@BSA samples in deionized water, and all samples were then heated for 5 min at each temperature (from 25°C to 100°C) with the intervals of 5°C. P_1M_5@BSA and P_1M_{10}@BSA sustained the transparent state (Figure 2B) and unchanged FTIR (P_1M_5@BSA as representative; Figure S5) along with the incubation in elevated temperature water, indicating the thermostability. In addition, cryo-electron microscope (Cryo-EM) revealed similar morphology for freshly prepared P_1M_5@BSA and 100°C-incubated P_1M_5@BSA (Figures 2C and 2D). In contrast, native BSA, P_2M_1@BSA, and P_1M_1@BSA displayed emulsion state (Figure 2B) and transformational morphologies (BSA as representative; Figures 2E, 2F, and S6) at high temperatures, implying denaturation and aggregation of proteins.

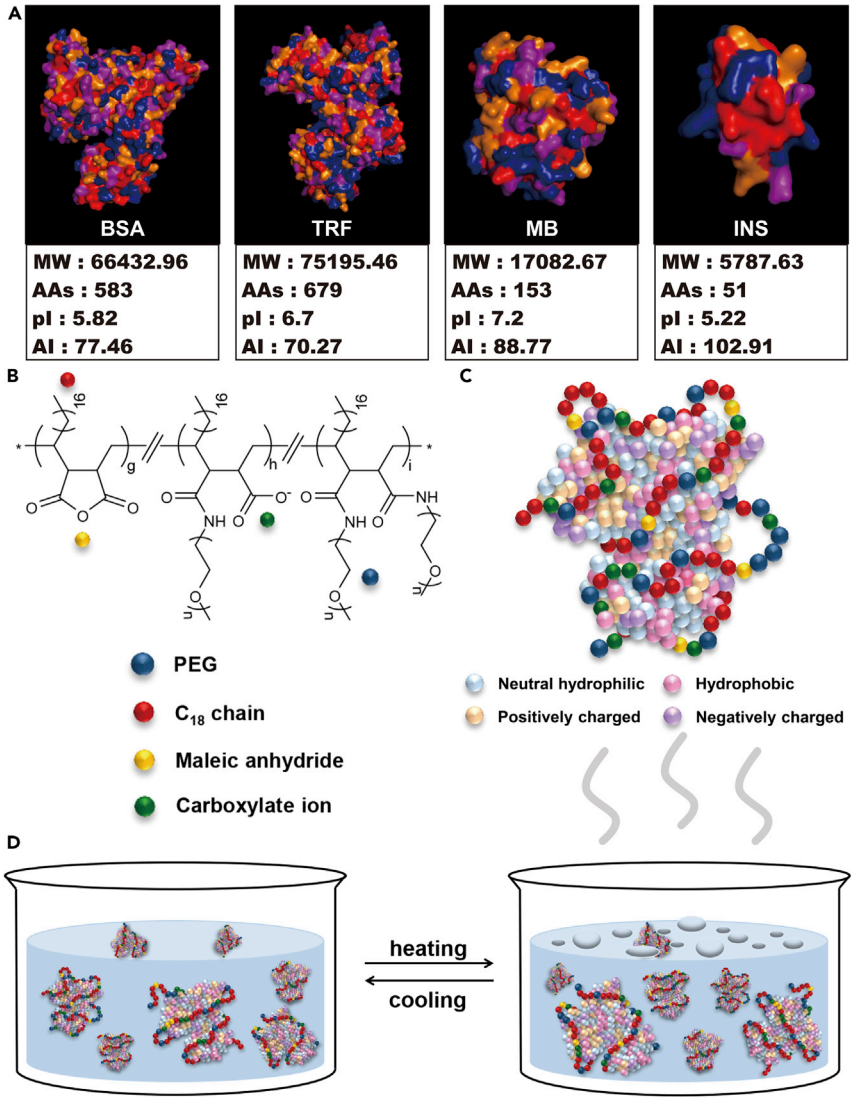

Figure 1. Interactions of amphiphilic polymers with mesophilic proteins

(A) The protein surfaces are analyzed and displayed chemically heterogeneous—BSA (PDB: 3V03), TRF (PDB: 4X1B), MB (PDB: 1DWS), and INS (PDB: 3I3Z) obtained from the Protein Data Bank. Blue, neutral hydrophilic; red, hydrophobic; orange, positively charged; purple, negatively charged. Molecular weight (MW), number of amine acids (AAs), theoretical pI (pI), and aliphatic index (AI) are retrieved from Expasy using ProtParam tool.

(B) Amphiphilic polymers with varied hydrophilicity and hydrophobicity.

(C) Graphical representation showing amphiphilic polymers function as chaperone-like effect to interact with proteins and stabilize proteins.

(D) Thermal stabilization of amphiphilic polymers offering with mesophilic proteins in hyperthermal water.

Far UV circular dichroism (FUCD) (Greenfield, 2006; Kelly et al., 2005) were then devoted to study the structural information of BSA and P_xM_y@BSA post-incubation at different temperatures. The FUCD spectrums for P_xM_y@BSA at 25°C without heating performed unimpaired negative characteristic peaks at 208 nm/222 nm and positive characteristic peak at 192 nm (Figure 2G; blue spectrums), in consistent with that of native BSA. This observation further demonstrated that BSA encapsulated with P_xM_y polymers exhibited the same structural characteristics as native BSA under ambient conditions (25°C, 1 atm.), agreeing well with the FTIR results in Figures 2A and S4, explaining that encapsulation, subsequent lyophilization, and redissolution had negligible influence on the secondary structures. However, increasing the temperature from 25°C to 100°C saw obvious differential intensity for BSA and P_xM_y@BSA with spectral characteristic at 192 nm, characteristic at 208 nm/222 nm (Figures 2G and S7A). The optimal P_1M_5@BSA and P_1M_{10}@BSA exhibited remarkable stability of secondary

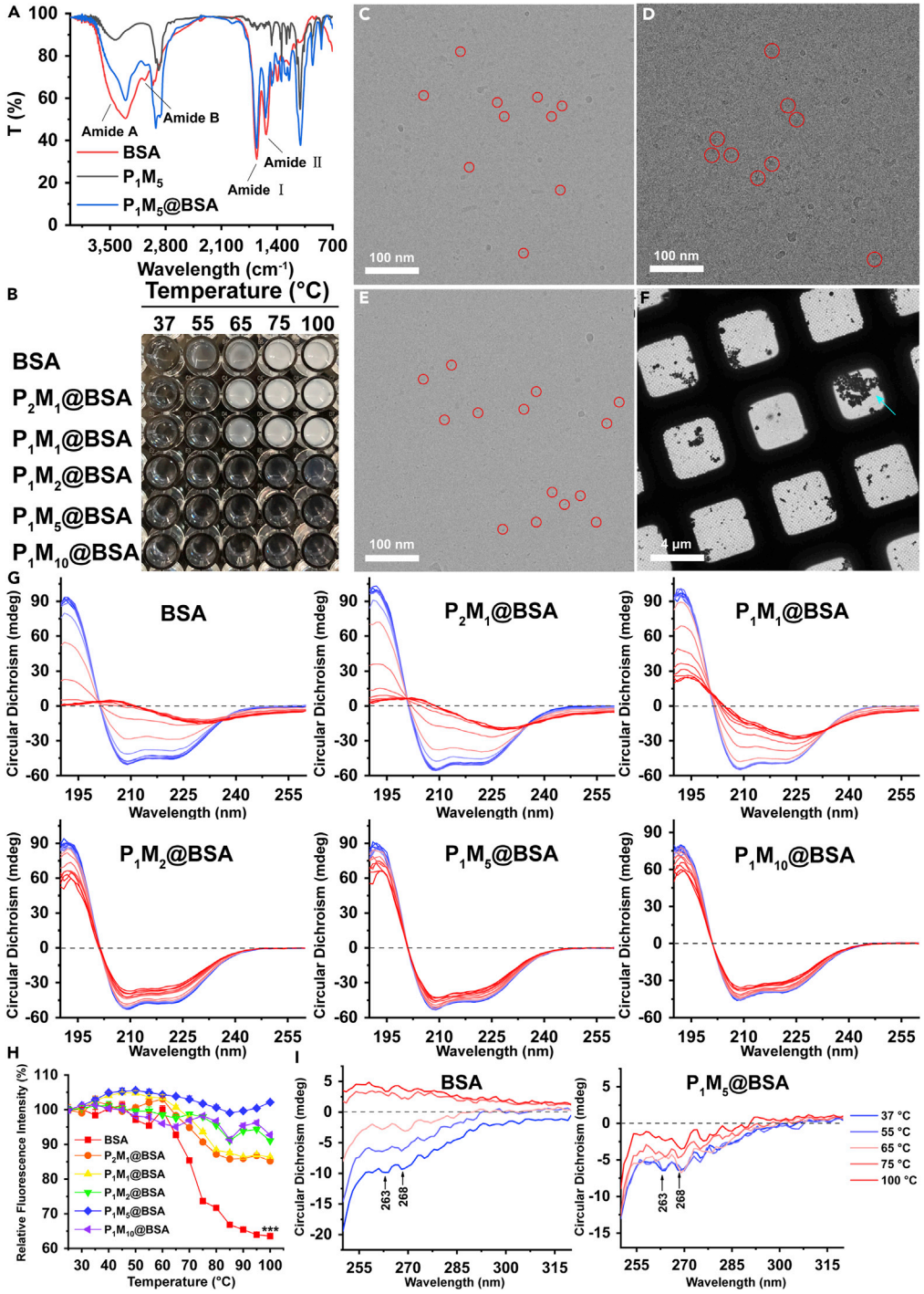

Figure 2. Thermostabilization of P_xM_y offering to mesophilic protein

(A) FTIR spectrums for native BSA (red), P_1M_5 (black), and P_1M_5@BSA (blue) without thermal treatment. The bands at 1653, 1535, 3500, and 3065 cm^{-1} correspond to amide I, amide II, amide A, and amide B groups in BSA.

(B) Visualization of BSA and P_xM_y@BSA after incubating in elevated temperature water.

(C–F) Cryo-EM images of BSA and P_1M_5@BSA after 25°C and 100°C treatment. (C) P_1M_5@BSA-25°C, (D) P_1M_5@BSA-100°C, (E) BSA-25°C, (F) BSA-100°C. Images (C), (D), and (E) were acquired under magnification of 120,000, whereas image (F) was acquired under magnification of 3,400. Particles of BSA and P_1M_5@BSA are indicated in red circles; aggregation of BSA alone after 100°C treatment is indicated with cyan arrow.

Figure 2. *Continued*

(G) Temperature-dependent FUCD spectrums for BSA, P_2M_1@BSA, P_1M_1@BSA, P_1M_2@BSA, P_1M_5@BSA, and P_1M_{10}@BSA, indicating changes of peak intensities in response to thermal treatment from 25°C (blue) to 100°C (red).

(H) Fluorescence intensity of BSA (red), P_2M_1@BSA (orange), P_1M_1@BSA (yellow), P_1M_2@BSA (green), P_1M_5@BSA (blue), and P_1M_{10}@BSA (purple) after thermal treatment from 25°C to 100°C (λ_{ew} = 345 nm, λ_{ex} = 280 nm). Data are shown as mean ± s.d. (n = 3). (***P < 0.001).

(I) Temperature-dependent NUCD spectrums of BSA and P_1M_5@BSA, indicating changes of tertiary structures in response to thermal treatment.

structures at elevated temperatures, as evidenced by stable intensity of the α-helical characteristic peaks at 208 nm/222 nm and stable intensity of β-sheets at characteristic peak 216 nm. Meanwhile, corresponding characteristic peaks of native BSA, P_2M_1@BSA, P_1M_1@BSA, and BSA with protective agent glycerin (Figures 2G and S7B) showed a dramatically reduction. This demonstrated that P_1M_5 and P_1M_{10} amphiphilic polymers hold much better thermal protection effect than classic protective agent, glycerin. Furthermore, the stable fluorescence emission at 345 nm from P_1M_5@BSA and P_1M_{10}@BSA (Figure 2H) derived from Trp residue, which is extremely sensitive to its surrounding microenvironment (Friedrichs, 1997), were detected after incubating at elevated temperatures, indicating reserved tertiary structures of BSA. Near UV circular dichroism (NUCD) for optimal P_1M_5@BSA (Figure 2I) also demonstrated the maintained tertiary structures, as evidenced by similar spectrums at 263 nm and 268 nm, referring to the asymmetry around disulfide bridges and the microenvironment of the tryptophan residue (Sun et al., 2005).

Retained structures after incubating with hyperthermia water

Closed examinations were undertaken on the BSA and P_xM_y@BSA to quantitatively analyze the temperature-dependent properties induced by thermal energy. The optimal P_1M_5@BSA retained its original secondary structures in hyperthermal water as reveled in the tendency chart (Figure 3A). Specifically, the total α-helical contents of native BSA was dropped by 66.1% (0.56 at 25°C to 0.19 at 70°C) in 70°C water, a concomitant increase of 188.9% β-sheets and 73.9% unordered contents (Table S2), whereas hyperthermia did not impact too much on the turn subunits. In contrast, only 6.7% and 5.8% reduction of α-helical contents were observed for P_1M_5@BSA and P_1M_{10}@BSA in 70°C water (Tables S6-S7). Significantly, 91.1% reduction of α-helical for native BSA was detected in 100°C water; meanwhile, only a slight of α-helices from P_1M_5@BSA (20% reduction) and P_1M_{10}@BSA (25% reduction) were transformed in 100°C water (Tables S2, S6, and S7). From these analyses it was evident that P_1M_5@BSA and P_1M_{10}@BSA had efficient protection of their secondary (Figures 3A and S8 and Tables S2–S7) and tertiary structures (Figures 2H and 2I) in hyperthermal environments, even in boiling water, opening the window to potential activities retention of mesophilic proteins beyond those in normal physiological conditions.

Structure-function relationship

The structure-function relationship of amphiphilic polymers and their thermal stabilization effect was investigated. All-atom classical molecular dynamics (MD) simulations of complexes (BSA with and without PEG or/and C_{18} fragment, respectively) were performed in Amber18 package to study the stability of protein backbone under the different temperatures (Bondanza et al., 2020; Jia et al., 2020). Final 100 ns trajectories were used for further analysis. MD of BSA alone in 100°C showed large root-mean-square deviation (RMSD) of ~4.0 Å in comparison with ~1.9 Å at 25°C, indicating that structural stability decreased at 100°C (Figure 3B). However, incorporation of C_{18} fragments into the system could significantly suppress the RMSD value of BSA at 100°C (deviation of ~3.5 Å), signifying that C_{18} fragments had the effect of stabilizing protein at high temperature (Figure 3C). Combinatorially incorporating C_{18} and PEG fragments into the BSA, RMSD value of the protein could further decrease at 100°C (deviation of ~3.3 Å), which indicates synergistic hyperthermia protection by C_{18} and PEG for BSA (Figure 3D). The experimental results also verified that PEG densities anchored on the polymers significantly impacted the stabilization effect; P_2M_1@BSA and P_1M_1@BSA with PEG densities to polymers at 100% and 50% were inclined to denature and aggregate under the treatment of hyperthermia (Figure 2G; middle and right of the first row), as high densities of hydrophilic PEG chains within the polymers (P_2M_1, P_1M_1) would weaken the stabilization of hydrophobic C_{18}. In contrast, P_1M_5@BSA and P_1M_{10}@BSA with optimal PEG densities to polymers at 20% and 10% (Figure 2G; middle and right of the second row) performed much more efficient thermal protection for BSA. In addition, the C_{18} chains also play a dominant responsibility to the stabilization function of amphiphilic polymers, evidenced by the polymers without C_{18} chains (PEG_1-PMH_5, PEG_1-PMH_{10}) that they had negligible protection effect (Figure 3E) as that of P_1M_5 and P_1M_{10} polymers.

In order to further investigate the binding properties between proteins and polymers, the binding free energy calculations were performed by the molecular mechanics/generalized born surface area (MM/GBSA) method.

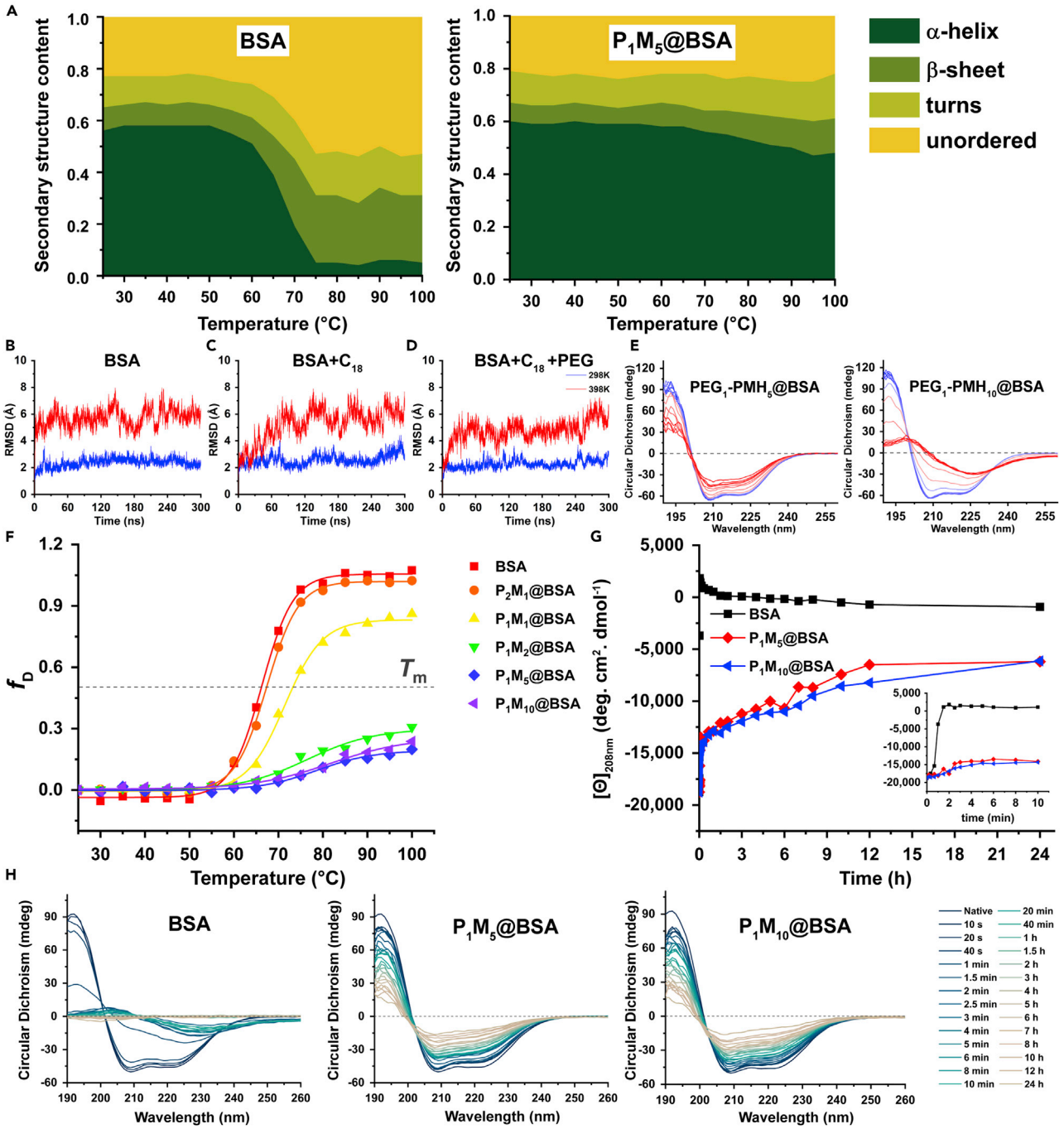

Figure 3. Temperature-dependent properties and long-term protection effect of P_1M_5 and P_1M_{10} with mesophilic protein

(A) Secondary structure contents of P_1M_5@BSA deconvoluted from FUCD spectrums using DichroWeb Service after various thermal treatment. The ordinate showed the proportion of various secondary structures to the total protein structures.

(B–D) Time evolution of root-mean-square deviation (RMSD) of BSA, BSA + C_{18}, and BSA + C_{18} + PEG exposed in the external electric fields with different temperature, 298 K (blue) and 398 K (red), respectively.

(E) Temperature-dependent FUCD spectrums for PEG_1-PMH_5@BSA and PEG_1-PMH_{10}@BSA, indicating changes of peak intensities in response to thermal treatment from 25°C (blue) to 100°C (red).

(F) Plots of fraction denatured (f_D) of BSA and P_xM_y@BSA to temperatures. Data are calculated from FUCD to draw a two-state model of denaturation and fitted with sigmoid functions (solid lines).

Figure 3. *Continued*

(G) Plots of mean residue ellipticity at 208 nm (to determine retained structure) against time after treatment for 0 to 24 h in 100°C water. BSA (black), P_1M_5@BSA (pink), and P_1M_{10}@BSA (red). Data in 10 min are shown in the inset.

(H) FUCD spectrums of BSA, P_1M_5@BSA, and P_1M_{10}@BSA after treatment from 0 (blue) to 24 h (pale yellow) in 100°C water.

At 298 K, the binding free energies of C_{18}, PEG, and C_{18} + PEG are −34.2 Kcal/mol, −210.6 Kcal/mol, and −104.6 Kcal/mol, respectively. Meanwhile, at 398 K, the binding free energies of C_{18}, PEG, and C_{18} + PEG are −33.9 Kcal/mol, −258.7 Kcal/mol, and −106.4 Kcal/mol, respectively (Figure S9 and Table S8). Those results indicate that PEG has higher binding tendency with protein but C_{18} with lower binding tendency at both 298 K and 398 K conditions. However, from the decomposition analysis, C_{18} and PEG binding to protein will dramatically disturb the region functions of 126–144 (Majorek et al., 2012); C_{18} + PEG without such region functions disordered will help to maintain protein functions, which is in agreement with our experimental data.

Thermodynamics investigation and protective duration

We then applied a two-state model by drawing plots of fraction denatured (f_D) against temperature to assess denaturation thermodynamics correlated with protein unfolding and denaturation. The denaturation curve of native BSA happened in a narrow temperature range (around 66°C; Figure 3F), suggesting a radical denaturation and aggregation process. In contrast, P_1M_5@BSA and P_1M_{10}@BSA exhibited a slow gradient pre-transition baseline below 100°C, referring to nearly intact secondary and tertiary structures. Specifically, native BSA, P_2M_1@BSA, P_1M_1@BSA, P_1M_2@BSA, P_1M_5@BSA, and P_1M_{10}@BSA had half denaturation T_m of 65.4°C, 62.3°C, 77.5°C, 127.1°C, 181.6°C, and 171.5°C (Table S9), respectively. As shown, P_1M_5@BSA and P_1M_{10}@BSA could greatly improve the thermostability for BSA by increasing T_m, which were 116.2°C and 106.1°C higher than that of native BSA. It is also suggested that hydrophilic PEG had synthetic effect to stabilize mesophilic proteins as described in Figures 2G and 3E, by tailoring the ratios of hydrophilic and hydrophobic units. To obtain the optimal protection of mesophilic proteins, the PEG should be a well-balanced design. Thermodynamic analysis uncovered intrinsic reasons for the increased thermostability of P_1M_5@BSA and P_1M_{10}@BSA in hyperthermal water. Remarkably, for P_1M_5@BSA and P_1M_{10}@BSA, the thermostability was rooted in a large reduced conformational entropy ΔS_m (33.9 and 33.3 $JK^{-1}mol^{-1}$) and enthalpy ΔH_m (6.2 and 5.7 kJ mol^{-1}) (Kazlauskas, 2018), compared with that of native BSA, P_2M_1@BSA, and P_1M_1@BSA (Figure S10 and Table S9). Meanwhile, the thermal protection of P_1M_2@BSA between them was as shown in Figures 2B and 2G and Table S9. We rationalize this as the high confinement and shielding abilities generated from the balanced hydrophobic effect of C_{18} and hydrophilic effect of PEG for P_1M_5@BSA and P_1M_{10}@BSA. Simultaneously, the non-covalent interactions are not strong enough to alter the secondary and tertiary structures of proteins.

In light of the thermal protection of P_1M_5 and P_1M_{10} offering with mesophilic proteins, the protective duration was evaluated. P_1M_5@BSA and P_1M_{10}@BSA were incubated in water of 55°C, 65°C, 75°C, and 100°C for different periods. P_1M_5@BSA and P_1M_{10}@BSA even with 24 h of treatment at 55°C showed no observable alteration of secondary structures (Figures S11A and S11D). On the contrary, 41.1% reduction of α-helices and 111.1% increment of β-sheets for native BSA were observed within 12 h of incubation at 55°C. In addition, native BSA was almost completely denatured with 1-h incubation at 65°C and 4-min' incubation at 75°C, whereas P_1M_5@BSA and P_1M_{10}@BSA showed long-term thermostability at these two high temperatures (Figures S11B, S11E, S11C, and S11F). Surprisingly, when P_1M_5@BSA and P_1M_{10}@BSA were incubated in boiling water for 24 h, 33.0% and 32.7% BSA maintained their structures; their half-denatured time in 100°C water was 6.64 h and 8.24 h (Figures 3G and 3H). In contrast, native BSA denatured in a very short time after incubation in 100°C water, with half denatured time of 50.8 s. We then investigated the long-term protective action of selected P_1M_5 at the room temperature. P_1M_5@BSA solutions retained the structural integrity of BSA in 2 weeks, whereas native BSA had a great loss of their 29.5% original structure in 2 weeks (Figure S12). This could be a great beneficial for the vaccine storage, as vaccine invalidates easily at room temperature and requires cold-chain transportation (Levin et al., 2007; Ohtake et al., 2011).

General protection effect to mesophilic proteins

Given the efficient thermal protection of the amphiphilic polymers for BSA, we then investigated if this could be a general method to protect mesophilic proteins in hyperthermal water. Essential proteins for mankind with various sizes and surface characteristics (insulin, myoglobin and transferrin), were also encapsulated by P_1M_5. All proteins encapsulated by P_1M_5 showed stable FUCD spectrums (Figures 4A–4F) and increased T_m (Table S10) after incubating in hyperthermal water, indicating the thermostability of

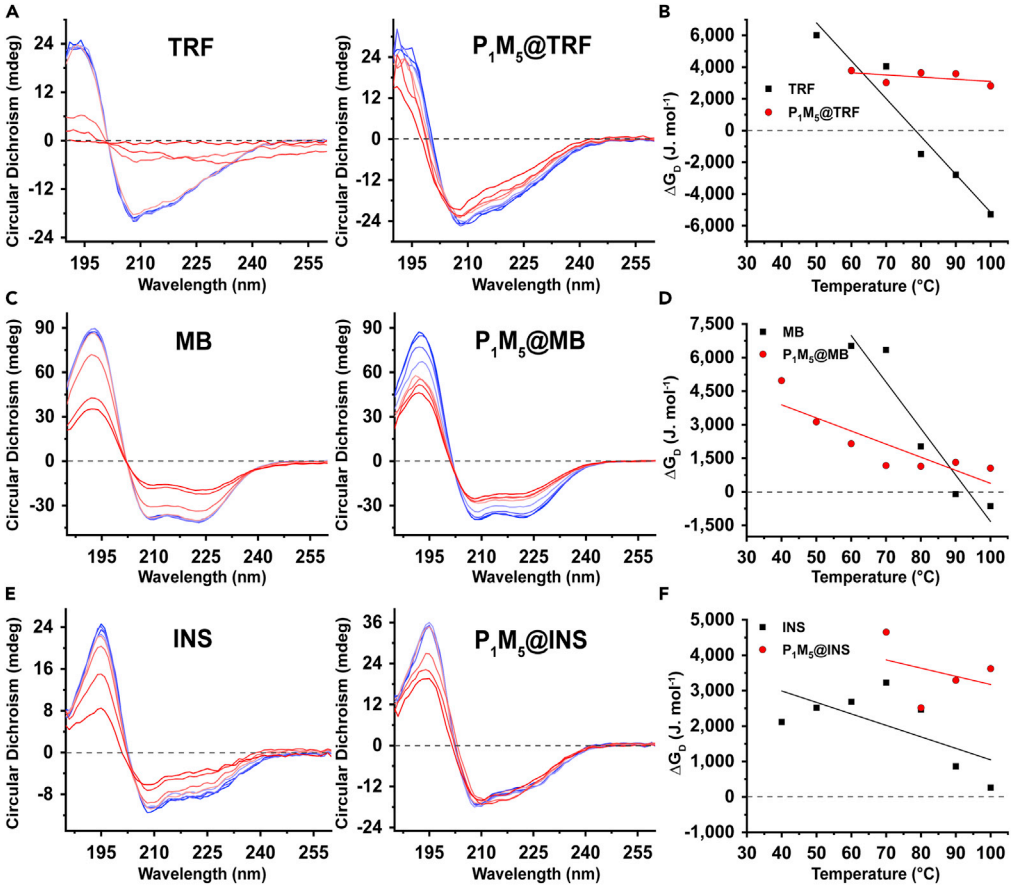

Figure 4. Thermal protection effect of P_1M_5 offering with other mesophilic proteins

(A) Temperature-dependent FUCD spectrums for TRF and P_1M_5@TRF after incubating for 5 min in hyperthermal water from 30°C (blue) to 100°C (red).

(B) Plots of free energy (ΔG_D) of denatured TRF against temperatures, showing transition region for TRF (black) and P_1M_5@TRF (red). Solid lines represent linear regression used to extract thermodynamic parameters.

(C) Temperature-dependent FUCD spectrums for MB and P_1M_5@MB after incubating for 1 h in hyperthermal water from 30°C (blue) to 100°C (red).

(D) Plots of free energy (ΔG_D) of denatured MB against temperatures, showing transition region for MB (black) and P_1M_5@MB (red). Solid lines represent linear regression used to extract thermodynamic parameters.

(E) Temperature-dependent FUCD spectrums for INS and P_1M_5@INS after incubating for 2 h in hyperthermal water from 30°C (blue) to 100°C (red).

(F) Plots of free energy (ΔG_D) of INS denaturation against temperature, showing transition region for INS (black) and P_1M_5@INS (red). Solid lines represent linear regression used to extract thermodynamic parameters.

P_1M_5@TRF, P_1M_5@MB, and P_1M_5@INS. Specifically, only 16.8%, 42.5%, and 11.4% secondary structures of P_1M_5@TRF, P_1M_5@MB, and P_1M_5@INS changed after incubating for 5 min, 1 h, and 2 h, respectively in boiling water (Figure S13). Interestingly, the T_m for P_1M_5@TRF increased to 326.6°C, compared with 78.4°C that of native TRF. In short, these results showed that P_1M_5 could greatly preserve the structures of mesophilic proteins under extreme conditions, regardless of their size, hydrophilicity, and electronegativity, providing a general method to stabilize mesophilic proteins in hyperthermal water.

CONCLUSIONS

In summary, our finding affords a general method to stabilize mesophilic proteins in hyperthermal water with retention of their secondary and tertiary structures. PEG and C_{18} chains anchored on the polymers impact the stabilization effect for mesophilic proteins. A wide range of mesophilic proteins encapsulated by the optimal amphiphilic polymers (P_1M_5 and P_1M_{10}) show dramatically increased T_m compared with native counterparts. It is anticipated that the ultra-strong thermal stabilization method for mesophilic

proteins presents great potential applications for protein translational application, including pharmaceutical vaccine storage free from cold-chain requirement and enzyme engineering at high temperatures.

Limitations of the study

In this study, we developed a general method to improve the thermostabilization of proteins. Specifically, we rationally designed and synthesized polymers that could self-assemble with proteins by analyzing the hydrophilicity, hydrophobicity, and electrostatic potential of proteins' surface. The polymer@protein complex obtained after self-assembly could significantly improve the structural stability and biological function stability of proteins in hyperthermal water. However, this protein protection method still needs more data to support its protection of protein biological activity in hyperthermal water, and the actual transformation of this method still needs further research.

METHODS

All methods can be found in the accompanying transparent methods supplemental file.

STAR★METHODS

Detailed methods are provided in the online version of this paper and include the following:

- RESOURCE AVAILABILITY
  - Lead contact
  - Materials availability
  - Data and code availability
- METHOD DETAILS
  - Materials
  - Analysis of proteins
  - Characterization of polymers, proteins, and polymer@protein
  - Molecular dynamics simulations
  - Synthesis of polymers
  - Preparation of polymer@protein complexes
  - Thermal stabilization of P_xM_y@complexes
  - Thermal denaturation thermodynamics
  - Long-term stabilization of P_xM_y@BSA at elevated temperatures
  - Long-term storage of P_1M_5@BSA at room temperature
  - Thermal stabilization of P_1M_5 for other mesophilic proteins
- STATISTICAL ANALYSIS

SUPPLEMENTAL INFORMATION

Supplemental information can be found online at https://doi.org/10.1016/j.isci.2021.102503.

ACKNOWLEDGMENTS

This work was supported by the startup funding from Jinan University, the Fundamental Research Funds for the Central Universities (No. 11618337), and National Natural Science Foundation of China (No. 81903546).

AUTHOR CONTRIBUTIONS

X.W. Liu designed the study; X.Q. Xin, Y.W. Xu, and H. Shi performed the experiments; X.Q. Xin analyzed the data; X.W. Liu and X.Q. Xin wrote the manuscript.

DECLARATION OF INTERESTS

The authors declare no competing interests.

Received: January 12, 2021
Revised: April 14, 2021
Accepted: April 29, 2021
Published: May 21, 2021

REFERENCES

Akhtar, M., and Ding, R. (2017). Covalently cross-linked proteins & polysaccharides: formation, characterisation and potential applications. Curr. Opin. Colloid Interf. Sci. *28*, 31–36.

Akram, M., Anwar, S., Bhat, I.A., and Kabir ud, D. (2017). Unraveling the interaction of hemoglobin with a biocompatible and cleavable oxy-diester-functionalized gemini surfactant. Int. J. Biol. Macromol. *96*, 474–484.

Arnold, F.H., and Volkov, A.A. (1999). Directed evolution of biocatalysts. Curr. Opin. Chem. Biol. *3*, 54–59.

Baker, S.L., Munasinghe, A., Murata, H., Lin, P., Matyjaszewski, K., Colina, C.M., and Russell, A.J. (2018). Intramolecular interactions of conjugated polymers mimic molecular chaperones to stabilize protein–polymer conjugates. Biomacromolecules *19*, 3798–3813.

Barth, A. (2007). Infrared spectroscopy of proteins. BBA - Bioenerg. *1767*, 1073–1101.

Bondanza, M., Cupellini, L., Faccioli, P., and Mennucci, B. (2020). Molecular mechanisms of activation in the orange carotenoid protein revealed by molecular dynamics. J. Am. Chem. Soc. *142*, 21829–21841.

Brogan, A.P.S., Bui-Le, L., and Hallett, J.P. (2018). Non-aqueous homogenous biocatalytic conversion of polysaccharides in ionic liquids using chemically modified glucosidase. Nat. Chem. *10*, 859–865.

Chang, Y.-C., and Bowie, J.U. (2014). Measuring membrane protein stability under native conditions. Proc. Natl. Acad. Sci. U S A *111*, 219.

Chen, J., Wang, J., Zhang, X., and Jin, Y. (2008). Microwave-assisted green synthesis of silver nanoparticles by carboxymethyl cellulose sodium and silver nitrate. Mater. Chem. Phys. *108*, 421–424.

Chu, K., Vojtchovsky, J., McMahon, B.H., Sweet, R.M., Berendzen, J., and Schlichting, I. (2000). Structure of a ligand-binding intermediate in wild-type carbonmonoxy myoglobin. Nature *403*, 921–923.

Cummings, C., Murata, H., Koepsel, R., and Russell, A.J. (2014). Dramatically increased pH and temperature stability of chymotrypsin using dual block polymer-based protein engineering. Biomacromolecules *15*, 763–771.

Eyles, S.J., Speir, J.P., Kruppa, G.H., Gierasch, L.M., and Kaltashov, I.A. (2000). Protein conformational stability probed by fourier transform ion cyclotron resonance mass spectrometry. J. Am. Chem. Soc. *122*, 495–500.

Friedrichs, B. (1997). Th. Peters. Jr.: All about Albumin. Biochemistry, Genetics, and Medical Applications (Academic Press, Inc.), p. 1996.

Gekko, K., and Timasheff, S.N. (1981). Mechanism of protein stabilization by glycerol: preferential hydration in glycerol-water mixtures. Biochemistry *20*, 4667–4676.

Greenfield, N.J. (2006). Using circular dichroism spectra to estimate protein secondary structure. Nat. Protoc. *1*, 2876–2890.

Hagemans, D., van Belzen, I.A., Moran Luengo, T., and Rudiger, S.G. (2015). A script to highlight hydrophobicity and charge on protein surfaces. Front. Mol. Biosci. *2*, 56.

Hannink, J.M., Cornelissen, J.J., Farrera, J.A., Foubert, P., De Schryver, F.C., Sommerdijk, N.A., and Nolte, R.J. (2001). Protein-polymer hybrid amphiphiles this research was supported by The Netherlands foundation for chemical research (CW-NWO), the EC TMR sisitomas and ESF smarton programs, and the ministerio de Educacion y cultura (Spain). Angew. Chem. Int. Ed. Engl. *40*, 4732–4734.

Huang, P.S., Boyken, S.E., and Baker, D. (2016). The coming of age of de novo protein design. Nature *537*, 320–327.

Imanaka, T., Shibazaki, M., and Takagi, M. (1986). A new way of enhancing the thermostability of proteases. Nature *324*, 695–697.

Jia, R., Martens, C., Shekhar, M., Pant, S., Pellowe, G.A., Lau, A.M., Findlay, H.E., Harris, N.J., Tajkhorshid, E., Booth, P.J., et al. (2020). Hydrogen-deuterium exchange mass spectrometry captures distinct dynamics upon substrate and inhibitor binding to a transporter. Nat. Commun. *11*, 6162.

Kazlauskas, R. (2018). Engineering more stable proteins. Chem. Soc. Rev. *47*, 9026–9045.

Ke, P.C., Pilkington, E.H., Sun, Y., Javed, I., Kakinen, A., Peng, G., Ding, F., and Davis, T.P. (2019). Mitigation of amyloidosis with nanomaterials. Adv. Mater. *32*, e1901690.

Kelly, S.M., Jess, T.J., and Price, N.C. (2005). How to study proteins by circular dichroism. Biochim. Biophys. Acta *1751*, 119–139.

Koepnick, B., Flatten, J., Husain, T., Ford, A., Silva, D.A., Bick, M.J., Bauer, A., Liu, G., Ishida, Y., Boykov, A., et al. (2019). De novo protein design by citizen scientists. Nature *570*, 390–394.

Kong, J., and Yu, S. (2007). Fourier transform infrared spectroscopic analysis of protein secondary structures. Acta Biochim. Biophys. Sin. *39*, 549–559.

Kong, X.T., Besteiro, L.V., Wang, Z., and Govorov, A.O. (2018). Plasmonic chirality and circular dichroism in bioassembled and nonbiological systems: theoretical background and recent progress. Adv. Mater. *32*, e1801790.

Lawrence, P.B., Gavrilov, Y., Matthews, S.S., Langlois, M.I., Shental-Bechor, D., Greenblatt, H.M., Pandey, B.K., Smith, M.S., Paxman, R., Torgerson, C.D., et al. (2014). Criteria for selecting PEGylation sites on proteins for higher thermodynamic and proteolytic stability. J. Am. Chem. Soc. *136*, 17547–17560.

Leuenberger, P., Ganscha, S., Kahraman, A., Cappelletti, V., Boersema, P.J., von Mering, C., Claassen, M., and Picotti, P. (2017). Cell-wide analysis of protein thermal unfolding reveals determinants of thermostability. Science *355*, eaai7825.

Levin, A., Levin, C., Kristensen, D., and Matthias, D. (2007). An economic evaluation of thermostable vaccines in Cambodia, Ghana and Bangladesh. Vaccine *25*, 6945–6957.

Liu, T., Wang, Y., Luo, X., Li, J., Reed, S.A., Xiao, H., Young, T.S., and Schultz, P.G. (2016). Enhancing protein stability with extended disulfide bonds. Proc. Natl. Acad. Sci. U S A *113*, 5910.

Liu, X., Tao, H., Yang, K., Zhang, S., Lee, S.-T., and Liu, Z. (2011). Optimization of surface chemistry on single-walled carbon nanotubes for in vivo photothermal ablation of tumors. Biomaterials *32*, 144–151.

Lopez-Garcia, P., Zivanovic, Y., Deschamps, P., and Moreira, D. (2015). Bacterial gene import and mesophilic adaptation in archaea. Nat. Rev. Microbiol. *13*, 447–456.

Ma, F.H., Li, C., Liu, Y., and Shi, L.Q. (2020). Mimicking molecular chaperones to regulate protein folding. Adv. Mater. *32*, e1805945.

Mahler, H.-C., Friess, W., Grauschopf, U., and Kiese, S. (2009). Protein aggregation: pathways, induction factors and analysis. J. Pharm. Sci. *98*, 2909–2934.

Majorek, K.A., Porebski, P.J., Dayal, A., Zimmerman, M.D., Jablonska, K., Stewart, A.J., Chruszcz, M., and Minor, W. (2012). Structural and immunologic characterization of bovine, horse, and rabbit serum albumins. Mol. Immunol. *52*, 174–182.

Martin, W., Baross, J., Kelley, D., and Russell, M.J. (2008). Hydrothermal vents and the origin of life. Nat. Rev. Microbiol. *6*, 805–814.

Matthews, B.W., Nicholson, H., and Becktel, W.J. (1987). Enhanced protein thermostability from site-directed mutations that decrease the entropy of unfolding. Proc. Natl. Acad. Sci. U S A *84*, 6663.

Mensink, M.A., Frijlink, H.W., van der Voort Maarschalk, K., and Hinrichs, W.L. (2017). How sugars protect proteins in the solid state and during drying (review): mechanisms of stabilization in relation to stress conditions. Eur. J. Pharm. Biopharm. *114*, 288–295.

Moffet, D.A., and Hecht, M.H. (2001). De novo proteins from combinatorial libraries. Chem. Rev. *101*, 3191–3204.

Monteith, W.B., Cohen, R.D., Smith, A.E., Guzman-Cisneros, E., and Pielak, G.J. (2015). Quinary structure modulates protein stability in cells. Proc. Natl. Acad. Sci. U S A *112*, 1739.

Mossuto, M.F., Bolognesi, B., Guixer, B., Dhulesia, A., Agostini, F., Kumita, J.R., Tartaglia, G.G., Dumoulin, M., Dobson, C.M., and Salvatella, X. (2011). Disulfide bonds reduce the toxicity of the amyloid fibrils formed by an extracellular protein. Angew. Chem. Int. Ed. Engl. *50*, 7048–7051.

Ni, J., Gao, Y.-Y., Tao, F., Liu, H.-Y., and Xu, P. (2018). Temperature-directed biocatalysis for the sustainable production of aromatic aldehydes or alcohols. Angew. Chem. Int. Ed. Engl. *57*, 1214–1217.

Ohtake, S., Martin, R., Saxena, A., Pham, B., Chiueh, G., Osorio, M., Kopecko, D., Xu, D., Lechuga-Ballesteros, D., and Truong-Le, V. (2011). Room temperature stabilization of oral, live attenuated Salmonella enterica serovar Typhi-vectored vaccines. Vaccine *29*, 2761–2771.

Razvi, A., and Scholtz, J.M. (2006). Lessons in stability from thermophilic proteins. Protein Sci. *15*, 1569–1578.

Rothschild, L.J., and Mancinelli, R.L. (2001). Life in extreme environments. Nature *409*, 1092–1101.

Satish, L., Millan, S., and Sahoo, H. (2019). Sustained activity and stability of lysozyme in aqueous ionic liquid solutions containing carboxymethylcellulose and polyethylene glycol. J. Mol. Liq. *278*, 329–334.

Schoene, C., Fierer, J.O., Bennett, S.P., and Howarth, M. (2014). SpyTag/SpyCatcher cyclization confers resilience to boiling on a mesophilic enzyme. Angew. Chem. Int. Ed. Engl. *53*, 6101–6104.

Scirè, A., Marabotti, A., Aurilia, V., Staiano, M., Ringhieri, P., Iozzino, L., Crescenzo, R., Tanfani, F., and D'Auria, S. (2008). Molecular strategies for protein stabilization: the case of a trehalose/maltose-binding protein from Thermus thermophilus. Proteins *73*, 839–850.

Smith, P.K., Krohn, R.I., Hermanson, G.T., Mallia, A.K., Gartner, F.H., Provenzano, M.D., Fujimoto, E.K., Goeke, N.M., Olson, B.J., and Klenk, D.C. (1985). Measurement of protein using bicinchoninic acid. Anal. Biochem. *150*, 76–85.

Sun, C., Yang, J., Wu, X., Huang, X., Wang, F., and Liu, S. (2005). Unfolding and refolding of bovine serum albumin induced by cetylpyridinium bromide. Biophys. J. *88*, 3518–3524.

Thomas, A.S., and Elcock, A.H. (2004). Molecular simulations suggest protein salt bridges are uniquely suited to life at high temperatures. J. Am. Chem. Soc. *126*, 2208–2214.

Timofeev, V.I., Chuprov-Netochin, R.N., Samigina, V.R., Bezuglov, V.V., Miroshnikov, K.A., and Kuranova, I.P. (2010). X-ray investigation of gene-engineered human insulin crystallized from a solution containing polysialic acid. Acta Crystallogr. Sect. F Struct. Biol. Cryst. Commun. *66*, 259–263.

Torres, M.P., Determan, A.S., Anderson, G.L., Mallapragada, S.K., and Narasimhan, B. (2007). Amphiphilic polyanhydrides for protein stabilization and release. Biomaterials *28*, 108–116.

Vieille, C., and Zeikus, G.J. (2001). Hyperthermophilic enzymes: sources, uses, and molecular mechanisms for thermostability. Microbiol. Mol. Biol. Rev. *65*, 1.

Wagoner, T.B., and Foegeding, E.A. (2017). Whey protein–pectin soluble complexes for beverage applications. Food Hydrocoll. *63*, 130–138.

Wang, G., Li, X., Mo, L., Song, Z., Chen, W., Deng, Y., Zhao, H., Qin, E., Qin, C., and Tang, R. (2012). Eggshell-inspired biomineralization generates vaccines that do not require refrigeration. Angew. Chem. Int. Ed. Engl. *51*, 10576–10579.

Wang, M., Lai, T.P., Wang, L., Zhang, H., Yang, N., Sadler, P.J., and Sun, H. (2015). "Anion clamp" allows flexible protein to impose coordination geometry on metal ions. ChemComm *51*, 7867–7870.

Watson, M.D., Monroe, J., and Raleigh, D.P. (2018). Size-dependent relationships between protein stability and thermal unfolding temperature have important implications for analysis of protein energetics and high-throughput assays of protein–ligand interactions. J. Phys. Chem. B *122*, 5278–5285.

Xiao, S., Patsalo, V., Shan, B., Bi, Y., Green, D.F., and Raleigh, D.P. (2013). Rational modification of protein stability by targeting surface sites leads to complicated results. Proc. Natl. Acad. Sci. U S A *110*, 11337.

STAR★METHODS

RESOURCE AVAILABILITY

Lead contact

Further information and requests should be directed to the lead contact, Doctor Xiaowen Liu (xwliu231@jnu.edu.cn).

Materials availability

Materials are available from the corresponding authors on request.

Data and code availability

This study did not generate computer code. All data and analytical methods are available in the main text or in supplemental information.

METHOD DETAILS

Materials

Poly(maleic anhydride-alt-1-octadecene) ($PMHC_{18}$, MW 30∼50 kDa), poly(ethylene-alt-maleic anhydride) (PMH, MW 100∼500 kDa), N-(3-dimethylaminopropyl)-N′-ethylcarbodiimide hydrochloride crystalline (EDC), holo-transferrin human (TRF), and myoglobin (MB) were purchased from Sigma-Aldrich. mPEG-NH_2 (MW ∼5 kDa) was purchased from Bomei Biotech. Co. Ltd. (Zhejiang, China). Recombinant human insulin (20 IU/mg) was purchased from Lijing Biochemical Technology Co. Ltd. (Shenzhen, China). Deuterated chloroform ($CDCl_3$) and bovine serum albumin (BSA) were purchased from J&K Scientific Ltd. BCA protein assay kit was obtained from Thermo Fisher Scientific Inc.

Analysis of proteins

Mesophilic proteins were analyzed with PyMOL (version 2.3.3). Crystal structures of BSA, TRF, MB, and INS—3V03 (Majorek et al., 2012), 4X1B (Wang et al., 2015), 1DWS (Chu et al., 2000), and 3I3Z (Timofeev et al., 2010), respectively—were obtained from the Protein Data Bank (PDB). PyMOL was used to simplify protein surfaces as neutral hydrophilic, hydrophobic, positively charged, or negatively charged patches (Hagemans et al., 2015). The Swiss-Prot/TrEMBL accession number obtained from corresponding protein database file—P02769 (BSA), P02787 (TRF), P68082 (MB) and P01308 (INS) —were used to retrieve protein related information (molecular weight, number of amino acids, theoretical pI, and aliphatic index) on Expasy by ProtParam tool (Chen et al., 2008).

Characterization of polymers, proteins, and polymer@protein

^1H NMR. All lyophilized polymers were required to be dissolved in deuterated chloroform ($CDCl_3$) and introduced into NMR tubes of 5 mm outer diameter. 1H NMR was performed by means of a Bruker DRX 300 NMR spectrometer (Karlsruhe, Germany) according to the standard pulse programs provided with the spectrometer (Figure S2).

Protein concentration determined by BCA. The protein concentrations in various polymer@protein complexes were determined with the BCA kit (Smith et al., 1985). The encapsulation efficiency (EE) and the loading content (LC) of polymer@ protein were then calculated using Equations (1) and (2), and an average 80%–90% of EE and 35%–45% of LC were achieved (Figures S3A and S3B).

$$EE\ (\%) = \text{amount of encapsulated proteins/total amount of proteins added} \times 100\% \quad \text{Equation (1)}$$

$$LC\ (\%) = \text{total weight of encapsulated proteins/total weight of complexes} \times 100\% \quad \text{Equation (2)}$$

Dynamic light scattering. Hydrodynamic diameters (Dh) of BSA and P_xM_y@BSA complexes in aqueous solution were determined by DLS. The DLS measurements were taken on a Nano S Zetasizer Nano Series instrument (Malvern, UK). The test temperature of the instrument was set to 25°C, and the equilibrium time was run for 120 s before each test. Each sample was tested for 6 times. The size of P_xM_y@BSA complexes determined was about 15–20 nm (Figure S3C).

Fourier transform infrared spectroscopy. FTIR was performed to study the secondary structures of proteins (Barth, 2007; Kong and Yu, 2007). Solutions of BSA and P_xM_y@BSA (BSA concentration, 1 mg/mL, 1 mL) with or without incubating at 100°C for 5 minutes were lyophilized before the FTIR test (Figures S4 and S5). The potassium bromide (KBr) tablets were made at mass ratio of 1: 100 (infrared sample: KBr), and then the KBr tablets were scanned on the sample stage. FTIR spectrums of the samples between wavelength 4000 cm^{-1} and 700 cm^{-1} were accumulated from 25 scans with a resolution of 2 cm^{-1}, data interval of 0.5 cm^{-1}, and a scan speed at 0.2 cm/s on a Frontier FTIR spectroscope (Perkin Elmer, USA). The bandwidth was 2 cm^{-1}.

Transmission electron microscopy. The morphology of the complexes was examined by TEM (JEOL, Japan). BSA or P_1M_5@BSA solution containing 0.3 mg/mL BSA with or without incubating at 100°C for 5 minutes was dropped onto a carbon-coated copper grid for three or four times and air-dried before observation at an acceleration voltage of 96 kV. As shown in Figure S6, after treatment in 100°C water, denatured BSA displayed a different morphology due to protein aggregation at high temperatures, whereas P_1M_5@BSA sustained the dispersive particle size around 20 nm.

Cryo-electron microscope. BSA or P1M5@BSA solution containing 0.3 mg/mL BSA with or without incubating at 100°C for 5 minutes. Then an FEI Vitrobot Mark IV plunger (FEI) was used for preparation of frozen-hydrated specimens. Three and half microlitres of BSA or P_1M_5@BSA was placed onto Quantifoil Cu R1.2/1.3 glow discharged 300 mesh holey carbon grids, which were then blotted for 3 seconds with blot force −1 to remove the excess solution before they were flash frozen in liquid ethane. The Vitrobot chamber was operated at constant 4°C and 100% humidity during blotting. The grids were transferred and stored in liquid nitrogen before data acquisition. Images were acquired on a 200 keV FEI Titan Krios electron microscope equipped with a Falcon3 direct electron counting camera at a nominal magnification of X120,000 (corresponding to a calibrated sampling of 1.25 Å per physical pixel). The images of BSA treated after 100°C were acquired under magnification of X3,400.

Far ultraviolet circular dichroism spectroscopy. FUCD spectrums were collected to investigate the secondary structures of proteins (Greenfield, 2006). The concentration of protein used to perform FUCD was determined by the lowest concentration at which it could receive integral circular dichroism signal. In this article, the concentrations used for BSA, TRF, MB, and INS were set at 0.3, 0.25, 0.2, and 0.2 mg/mL, respectively. The samples were kept in 1 mm quartz cuvettes at 25°C. FUCD spectrums were then collected on a Chirascan spectrometer (Applied Photophysics, UK) over a wavelength range of 190 to 260 nm for BSA and TRF and a wavelength range of 185 to 260 nm for MB and INS with 1 nm step. FUCD spectrums were deconvoluted to evaluate contents of secondary structure using the DichroWeb Service (UK) (Brogan et al., 2018), by converting the original excel file into a corresponding txt file and then submitting it to the server for calculation (Tables S2–S7). NRMSD represents the difference between the measured FUCD signal and the system fitted FUCD signal. NMRSD<0.05 is considered reasonable.

Fluorescence spectroscopy. BSA endogenous fluorescence intensity was evaluated using a multifunctional microplate reader system (BioTek). Protein solutions (1μM, 200 μL) were added to 96-well plates and excited at an excitation wavelength of 280 nm. Emission spectrums were collected at wavelength of 345 nm. Measurements were conducted at room temperature, and each sample was tested for three times.

Near ultraviolet circular dichroism (NUCD) spectroscopy. NUCD spectrums of BSA samples were to explain the changes of tertiary structures (Sun et al., 2005). The concentration of protein used to

detect NUCD spectra was determined by about five times of FUCD. BSA and P1M5@BSA (BSA concentration, 1 mg/mL, 2 mL) were incubated for five minutes in 37, 55, 65, 75, and 100°C water. All samples were then placed at room temperature overnight, and NUCD spectrums were collected on a Chirascan spectrometer (Applied Photophysics, UK) over a wavelength range of 250 to 320 nm for BSA with 1 nm step. The samples were run in 1 cm quartz cuvettes at 25°C.

Photograph of polymer@ protein complexes. To visualize protein aggregation in hyperthermia water, BSA and PxMy@BSA solutions (BSA, 1mg/mL, 200 μL) were incubated for 5 min with a metal bath in 37, 55, 65, 75, and 100°C water, respectively. Samples were then transferred to a 96-well plate and photographed, with the horizontal axis representing different samples (BSA, P_2M_1@BSA, P_1M_1@BSA, P_1M_2@BSA, P_1M_5@BSA, and P_1M_{10}@BSA) and the vertical axis representing different temperatures.

Molecular dynamics simulations

First of all, fragment unit parameters of C_{18}, PEG, and C_{18}+PEG were prepared based on Gaussian 09 software with b3lyp/6-31+g* level. Secondly, we built a box with the size of 80Å×80Å×80Å. The protein was added into the box and made sure the protein was located at the box center. After above steps, polymer fragments were randomly added into box. The all-atom classical molecular dynamics (MD) simulations were carried out with the Amber18 package. Force field parameters for C_{18} and PEG fragments were generated at the B3LYP/6-31+g(d) optimized geometry by the Gaussian 09 package. Amber ff14SB and Tip3p water parameters were selected to describe the protein and water molecules. During MD simulations, energy minimizations were performed using a combination of steepest descent and conjugate gradient algorithms. The periodic boundary conditions were used at the time step of 2 fs. All simulations were performed in the NPT ensemble. The minimum distance between solute and the periodic box edge was set to be 10 Å. All bonds involving hydrogens were fixed with the SHAKE algorithm. The temperature was kept constant using a Langevin thermostat at 300 K with a collision frequency of 2 ps^{-1}. The pressure was controlled by a Berendsen barostat at 1 bar with a relaxation time of 1 ps. The electrostatic term was computed using the Particle-Mesh-Ewald summation method. The cutoff algorithm was set as 10 Å. Finally, in current study, total 300 ns trajectory was collected for each system.

Synthesis of polymers

Amphiphilic polymers (P_2M_1, P_1M_1, P_1M_2, P_1M_5, and P_1M_{10}) were synthesized following our precious protocol (Liu et al., 2011) with a slight modification by grafting reaction of anhydride groups on $PMHC_{18}$ with PEG-NH_2 as described in Figure S1. Specifically, for polymers (P_2M_1 and P_1M_1) with high-density PEG chains, poly (maleic anhydride-alt-1-octadecene) ($PMHC_{18}$) dissolved in dichloromethane was first reacted with mPEG-NH_2 for 12 h (5 kDa, PEG: MHC_{18} monomer=2:1, 1:1 respectively) in the presence of 4 eq. triethylamine, and then 3 eq. N-(3-Dimethylaminopropyl)-N′-ethylcarbodiimide hydrochloride (EDC) was added to activate the generating carboxyl group and reacted for another 12 h. For polymers (P_1M_2, P_1M_5, and P_1M_{10}) with lower PEG chain densities, $PMHC_{18}$ dissolved in dichloromethane were reacted with mPEG-NH_2 for 24 h (5 kDa, PEG: MHC_{18} monomer=1:10, 1:5 and 1:2, respectively) in the presence of 4 eq. triethylamine. All the reaction solutions were then blown-dry by nitrogen. The obtained white solid products were reconstituted with deionized water, wherein the polymers with lower PEG densities required a slight of DMSO as cosolvent. The amphiphilic polymer solutions were then dialyzed against water using a 14 kDa cut-off membrane and then lyophilized. The final products were marked as P_xM_y with x units of PEG and y monomer units of $PMHC_{18}$ (e.g. P_1M_{10} represented a copolymer with 1 units of PEG and 10 monomer units of $PMHC_{18}$). The actual PEGylation ratios were determined by NMR analysis (Figure S2 and Table S1).

PEG_1-PMH_5 and PEG_1-PMH_{10} without C_{18} chains were analogously synthesized following the synthesis procedure of P_xM_y.

Preparation of polymer@protein complexes

P_xM_y@BSA complexes. The amphiphilic polymers (P_2M_1, P_1M_1, P_1M_2, P_1M_5, and P_1M_{10}) were respectively dissolved in deionized water and dropwise added to the BSA solution with mass ratios of 2:1 (polymers: BSA). After stirring for 2 h, the solutions were dialyzed against water using a 100 kDa cut-off membrane to remove unbound proteins or polymers and then lyophilized for storage.

P_1M_5@TRF complexes. P_1M_5@TRF complexes were prepared following abovementioned BSA encapsulation procedure.

P_1M_5@MB complexes. P_1M_5@MB complexes were prepared following abovementioned BSA encapsulation procedure with a slight modification; here P_1M_5@MB complexes were purified by dialysis with a 30 kDa cut-off membrane.

P_1M_5@INS complexes. Insulin was dissolved in 10 mM hydrochloric acid (pH 2.0), and the pH was subsequently adjusted to 8.0. The P_1M_5 aqueous solution was dropwise added to the insulin solution at mass ratios of 2:1 (polymers: insulin). After stirring for 2 h, the solution was dialyzed against water using a 14 kDa cut-off membrane to remove unbound insulin or polymers and lyophilized for storage.

PEG_1-PMH_5@BSA/ PEG_1-PMH_{10}@BSA complexes. The amphiphilic polymers (PEG_1-PMH_5 and PEG_1-PMH_{10}) were respectively dissolved in deionized water and dropwise added to the BSA solution with mass ratios of 2:1 (polymers: BSA). After stirring for 2 h, the solution was dialyzed against water using a 100 kDa cut-off membrane to remove unbound proteins or polymers and lyophilized for storage.

Thermal stabilization of P_xM_y@complexes

The BSA concentrations of the five samples (P_2M_1@BSA, P_1M_1@BSA, P_1M_2@BSA, P_1M_5@BSA, and P_1M_{10}@BSA) and control group (native BSA) were quantified to 0.3 mg/mL, and then these six groups were packed into EP tubes (500 μL/tube), in quadruplicate. These samples were incubated for 5 min at each temperature on a metal bath from 25°C to 100°C with intervals of 5°C. All samples were then placed at room temperature overnight, the secondary structures studied by FUCD (Figures S7A and S8) and fluorescence intensity at 345 nm of BSA were determined to confirm the optimal polymer with thermal protection of BSA. The BSA in 10% and 50% glycerin (10% and 50% represent the volume ratios of glycerin to water solution) were set as positive control groups (Gekko and Timasheff, 1981) (Figure S7B).

PEG_1-PMH_5@BSA and PEG_1-PMH_{10}@BSA without C_{18} chain were treated the same as P_xM_y@BSA to study the structure-function relationship.

Thermal denaturation thermodynamics

Thermodynamic indexes were evaluated by applying a two-state model by drawing fraction denatured (f_D) to the denaturation temperature (Brogan et al., 2018). Briefly, the denaturation process is described as an equilibrium between the denatured state (D) and the native state (N) at each temperature, where the ratio of each state is defined as the equilibrium constant for denaturation (K_D). K_D was calculated by using established methodology as described in the following. f_D for BSA was determined by the intensity of characteristic peak of FUCD at 208 nm (Characteristic peaks for TRF, MB, and INS were at 208 nm, 222 nm, and 208 nm, respectively);

$$f_D = (y - y_N)/(y_D - y_N)$$

where y_N is defined as the intensity of the 208 nm peak in the native state, and y_D is the intensity of the 208 nm peak in the denatured state. This allows for the expression of K_D; thus $K_D = f_D/(1 - f_D)$, where the Gibbs free energy of denaturation (ΔG_D) can be determined:

$$\Delta G_D = -RT\ln K_D$$

ΔG_D was plotted as a function of temperature, and the transition region was fitted using linear regression. When $\Delta G_D = 0$, the whole process was in equilibrium according to the two-state model, giving the following formula:

$$\Delta G_D = 0 = \Delta H_m - T_m \Delta S_m$$

From these plots, the entropy (ΔS_m) and enthalpy (ΔH_m) at the half-denaturation temperature (T_m) were evaluated according to the slope and the y-intercept, and the half-denaturation temperature was evaluated from the x-axis intercept.

Long-term stabilization of P_xM_y@BSA at elevated temperatures

The long-term protection effect for the optimal polymer (P_1M_5 and P_1M_{10}) was evaluated. The BSA concentrations of P_1M_5@BSA, P_1M_{10}@BSA, and the control group (BSA) were quantified to 0.3 mg/mL, then these three paralleled groups were packed into EP tubes (500 μL/tube). These samples were incubated on a metal bath at temperatures of 55°C, 65°C (T_m of BSA), 75°C, and 100°C, respectively. For thermal treatment at 55°C and 65°C, samples were incubated for 5, 10, 20, and 40 min and 1, 1.5, 2, 3, 4, 5, 6, 8, 10, 12, and 24 h, respectively. For thermal treatment at 75°C and 100°C, samples were incubated for 10, 20, and 40 seconds; 1, 1.5, 2, 2.5, 3, 4, 5, 6, 8, 10, 20, and 40 min; and 1, 1.5, 2, 3, 4, 5, 6, 7, 8, 10, 12, and 24 h, respectively. All samples were then placed at room temperature overnight, and the secondary structures of each sample were determined by circular dichroism spectroscopy (Figures S11A–S11C). The remaining secondary structures after different period's incubation at each temperature were calculated from plot of $[\theta]_{208nm\text{-}t}$ (Figures S11D–S11F); for example, the remaining secondary structures after 24 h of incubation at 100°C were calculated using the following formula:

$$\text{The secondary structure maintained (\%)} = ([\theta]_{208nm(100^\circ C,\ 24h)}/[\theta]_{208nm(100^\circ C,\ 0h)}) \times 100\%$$

The half-denatured time in100°C water was obtained from Figure 3F by taken point $[\theta]_{208nm(100^\circ C,\ 0h)/2}$ on the vertical axis and extended it to intersect the curve $[\theta]_{208nm\text{-}t}$ at 100°C; the abscissa of the intersection is the required value.

Long-term storage of P_1M_5@BSA at room temperature

To investigate the long-term storage of proteins for optimal polymer (P_1M_5), we stored the P_1M_5@BSA at room temperature for extended periods. The BSA concentration of P_1M_5@BSA and the control group (BSA) was adjusted to 0.3 mg/mL and then were packed into 50 mL EP tubes (20 mL/tube). These samples were stored at room temperature; the remaining secondary structures after 1, 2, 3, 4, 5, 6, 7, 14, 21, 30, 45, and 60 days of storage were evaluated by circular dichroism spectroscopy (Figures S12A and S12B).

Thermal stabilization of P_1M_5 for other mesophilic proteins

To explore whether this could be a general method for thermal protection of mesophilic proteins, the protective effect of P_1M_5 on TRF, MB, and INS in hyperthermal water were evaluated in a similar way as BSA. The concentration of native TRF and P_1M_5@TRF was adjusted to 0.25 mg/mL and treated for 5 min with a metal bath at each temperature from 30°C to 100°C at intervals of 10°C. The concentration of native MB and P_1M_5@MB was adjusted to 0.2 mg/mL and treated for 1 h with a metal bath at each temperature from 30°C to 100°C at intervals of 10°C. The concentration of native INS and P_1M_5@INS was adjusted to 0.2 mg/mL and treated for 2 h with a metal bath at each temperature from 30°C to 100°C at intervals of 10°C. After the thermal treatment, all samples were then placed at room temperature overnight, and the secondary structures of proteins were determined by circular dichroism spectroscopy over a wavelength range of 190–260 nm (TRF), 185–260 nm (MB), and 185–260 nm (INS). The secondary structures changed at each temperature was calculated from Figure S13 using the following formula (100°C) as example (characteristic peaks for TRF, MB, and INS were at 208 nm, 222 nm, and 208 nm, respectively):

$$\text{The secondary structure changed at 100°C (\%)} = (([\theta]_{208nm/222nm(25^\circ C)}\text{-}[\theta]_{208nm/222nm(100^\circ C)})/ [\theta]_{208nm/222nm(25^\circ C)}) \times 100\%.$$

STATISTICAL ANALYSIS

All results are expressed as mean ± s.d., mean ± s.e.m. as indicated, processed by Origin version 2018 for Windows (Origin Software, USA). Comparisons among all groups were evaluated using one-way ANOVA by Graph-Pad Prism version 7.0 for Windows (GraphPad Software, USA), and $P < 0.05$ was considered to be statistically significant. The statistical details of experiments can be found in the legends of Figures 2, S3, and S7.